Extension of the Bending-Gradient theory to thick plates buckling: application to Cross-Laminated-Timber panels

Olivier Perret, Arthur Lebée, Cyril Douthe, Karam Sab

Extension de la théorie du Bending-Gradient au voilement de plaques épaisses: application aux panneaux de bois lamellé-croisé

Extension of the Bending-Gradient theory to thick plates buckling: application to Cross-Laminated-Timber panels

Olivier Perret[1], **Arthur Lebée**[1], **Cyril Douthe**[2], **Karam Sab**[1]

1 : Université Paris-Est
Laboratoire Navier UMR 8205 CNRS, ENPC, IFSTTAR
6-8 Avenue Blaise Pascal, Cité Descartes, Champs-sur-Marne F- 77455 Marne-la-Vallée
e-mail : olivier.perret@enpc.fr, arthur.lebee@enpc.fr, karam.sab@enpc.fr

2 : Université Paris-Est
IFSTTAR, MAST
14-20 Boulevard Newton, Cité Descartes, Champs-sur-Marne F- 77455 Marne-la-Vallée Cedex 2
e-mail : cyril.douthe@ifsttar.fr

Résumé

Dans cet article, la résolution du problème de flambement linéaire est présentée en utilisant la théorie du Bending-Gradient, qui est une extension de la théorie de plaque de Reissner au cas des plaques hétérogènes. Les résultats de référence sont issus d'une étude numérique 3D par éléments finis avec une application au cas des panneaux de bois lamellé-croisé, des stratifiés épais et fortement anisotropes. Les résultats montrent, pour différentes géométries de plaques, que la théorie du Bending-Gradient estime précisément la charge critique des panneaux de bois lamellé-croisé contrairement aux théories classiques de Kirchhoff et de Reissner. De plus, il est démontré que la projection suggérée de la théorie du Bending-Gradient sur un modèle de Reissner donne des résultats très précis et pourrait donc avantageusement permettre le développement d'outils pour l'ingénieur en prenant en compte convenablement les effets de cisaillement.

Abstract

In this paper, the resolution of the linear buckling problem is presented using the Bending-Gradient theory which is an extension of the Reissner's plate theory to the case of heterogeneous plates. Reference results are taken from a 3D numerical analysis using finite-elements and applied to Cross-Laminated-Timber panels which are thick and highly anisotropic laminates. It is shown that for varying plate geometries, the Bending-Gradient theory predicts precisely the critical load of CLT panels contrary to classical Kirchhoff and first order shear deformation theories. Moreover, it is demonstrated that the suggested projection of the Bending-Gradient on a Reissner model gives very accurate results and could favorably allow the development of engineering tools which estimate properly shear effects.

Mots Clés: Théorie du Bending-Gradient, Flambement linéaire de plaque, Bois lamellé-croisé, Cisaillement roulant, Contraste de raideur

Keywords: Bending-Gradient Theory, Linear Plate Buckling, Cross Laminated Timber, Rolling Shear, Stiffness contrast

1 Introduction

Cross Laminated Timber (CLT) is an innovative wooden structural product which consists in several lumber layers stacked crosswise and glued on their wide faces. CLT constructions are assembled relatively quickly compared to buildings in steel or concrete and combines a low self weight and high membrane and bending stiffnesses. These attributes make it competitive in the prefabricated structures field with a low environmental impact. CLT panels are classically used in walls, floors and roofs as load carrying plate elements.

During the last twenty years, CLT buildings have gained in popularity and have grown higher and higher. As an exemple, the building Stadthaus, at Murray Grove in London, is the tallest modern timber building in the world. This nine-storey building is entirely designed in CLT except for the first

floor. The size-increasing of CLT buildings leads to high compressive stresses in bearing walls which could lead to buckling. Indeed in timber, the shear stiffness between radial and tangential directions, called also rolling shear, is two hundred times lower than the stiffness in fibers' direction. As rolling shear is sollicited in cross layers during buckling, taking it into account seems mandatory with such contrast.

Since, one of the dimension of CLT panels, the thickness, is significantly lower than the others, plate theories are appropriate to model CLT panels. The classical theory of plates, also known as Kirchhoff-Love [1] plate theory, is based on the assumption that the normal to the mid-plane of the plate remains normal after transformation neglecting thus the out-of-plane shear strain. It is the most commonly used theory to consider thin plates buckling [2]. When increasing the thickness, shear effects become more significant and the Kirchhoff model loses accuracy. The first order shear deformation theory (FOSDT), also called Reissner-Mindlin theory, considers a uniform shear strain distibution across thickness, and is often associated with the shear correction factor κ, set to $\frac{5}{6}$ by Reissner [3]. Several improvements of this theory have been suggested by considering higher order shear deformation distributions since the FOSDT loses efficiency in the field of laminated composites. Nevertheless, these theories lead to a discontinuous shear stress at interfaces whereas it is continuous in actual structures.

Murakami [4] overcomes this diffulty by suggesting a zig-zag theory which allows the shear stress continuity at layers' interface. Refinements of this theory were developped by modifying the displacement distribution across thickness. Although the zig-zag theories are very accurate for laminated composites, they are generally restricted to some specific configurations.

Lebée and Sab [5] suggests an improvement of the Reissner-Mindlin theory by considering the gradient of the bending moment to describe the shear behavior of the plate. The so-called Bending-Gradient (BG) theory presents excellent results for the cylindrical bending of laminates [6]. The main aspects of this theory are recalled in this paper and an extension to plate buckling is proposed.

First, in section 2, the Bending-Gradient theory is recalled and extended to the problem of stability. A projection on a simplified Reissner model is also discussed. Then, in section 3, a 3D numerical study is conducted and provides reference results. Finally, analytic results from the Bending-Gradient theory and more classical models are compared with reference results in section 4.

2 Linear buckling of plates with the Bending-Gradient theory

2.1 Notations

Vectors and higher-order tensors, up to sixth order, are used in the following. When using short notation, several underlining styles are used: vectors are straight underlined, $\underline{\boldsymbol{u}}$. Second order tensors are underlined with a tilde: $\underset{\sim}{\boldsymbol{M}}$ and $\underset{\sim}{\boldsymbol{\sigma}}$. Third order tensors are underlined with a parenthesis: $\underset{\frown}{\boldsymbol{R}}$ and $\underset{\frown}{\boldsymbol{\Gamma}}$. Fourth order tensors are doubly underlined with a tilde: $\underset{\approx}{\boldsymbol{D}}$ and $\underset{\approx}{\boldsymbol{C}^{\sigma}}$. Sixth order tensors are doubly underlined with a parenthesis: $\underset{\frown}{\underset{\approx}{\boldsymbol{f}}}$. The full notation with indices is also used. Then we follow Einstein's notation on repeated indices. Furthermore, Greek indices $\alpha,\beta,\delta,\gamma = 1,2$ denotes in-plane dimensions and Latin indices $i,j,k,l = 1,2,3$, all three dimensions.

The transpose operation ${}^{T}\bullet$ is applied to any order tensors as follows: $({}^{T}a)_{\alpha\beta\ldots\psi\omega} = a_{\omega\psi\ldots\beta\alpha}$. Three contraction products are defined, the usual dot product ($\underline{\boldsymbol{a}} \cdot \underline{\boldsymbol{b}} = a_i b_i$), the double contraction product ($\underset{\sim}{\boldsymbol{a}} : \underset{\sim}{\boldsymbol{b}} = a_{ij} b_{ji}$) and a triple contraction product ($\underset{\frown}{\boldsymbol{a}} \vdots \underset{\frown}{\boldsymbol{b}} = a_{\alpha\beta\gamma} b_{\gamma\beta\alpha}$). It should be noticed that closest indices are summed together in contraction products. The derivation operator $\underline{\boldsymbol{\nabla}}$ is also formally represented as a vector: $\underset{\sim}{\boldsymbol{a}} \cdot \underline{\boldsymbol{\nabla}} = a_{ij}\nabla_j = a_{ij,j}$ is the divergence and $\underset{\sim}{\boldsymbol{a}} \otimes \underline{\boldsymbol{\nabla}} = a_{ij}\nabla_k = a_{ij,k}$ is the gradient. Here $\otimes$ is the dyadic product.

Finally, Voigt notation $[\bullet]$ turns contraction products into conventional matrix products in order to ease comprehension.

2.2 The Bending-Gradient theory

Full details about the Bending-Gradient theory are provided in [5][6]. In the general case, membrane and bending parts of the problem are studied together but it is shown in the following section that the buckling problem can be solved considering only the bending part of the problem.

2.2.1 Generalized stress and strain fields

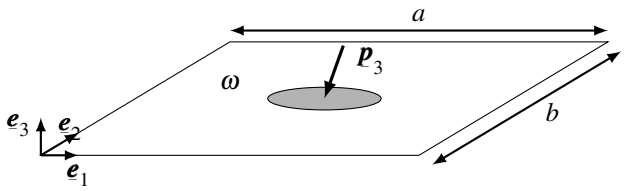

Fig. 1: 2D rectangular plate under out-of-plane external load

We consider a linear elastic rectangular plate of length a, width b and thickness h, which mid-plane is the 2D domain $\omega = ([0,a],[0,b])$. The 3D domain is then defined as $\Omega = \omega \times [-h/2, h/2]$. Cartesian coordinates x_1, x_2, x_3 are used in the reference frame $(\underline{e}_1, \underline{e}_2, \underline{e}_3)$. For a plate which constitutive material follows monoclinic symmetry according to ω, the membrane part and the bending part of the problem are uncoupled. Thus, the conventional generalized stresses for plates are defined from the 3D stress field σ_{ij} as follows:

$$\begin{cases} M_{\alpha\beta} = \displaystyle\int_{-\frac{h}{2}}^{\frac{h}{2}} x_3 \sigma_{\alpha\beta} dx_3 & \text{on } \omega \quad (1a) \\ Q_\alpha = \displaystyle\int_{-\frac{h}{2}}^{\frac{h}{2}} \sigma_{\alpha 3} dx_3 & \text{on } \omega \quad (1b) \end{cases}$$

where $M_{\alpha\beta}$ is the bending moment and Q_α the shear force. $\underline{\underline{\boldsymbol{M}}}$ follows the classical symmetry of stress tensors: $M_{\alpha\beta} = M_{\beta\alpha}$. Moreover, an additional static unknown is introduced: the generalized shear force $R_{\alpha\beta\gamma} = M_{\alpha\beta,\gamma}$. The 2D third-order tensor $\underline{\underline{\underline{\boldsymbol{R}}}}$ complies with the following symmetry: $R_{\alpha\beta\gamma} = R_{\beta\alpha\gamma}$. It is possible to derive the shear force $\underline{\boldsymbol{Q}}$ from $\underline{\underline{\underline{\boldsymbol{R}}}}$ with: $Q_\alpha = R_{\alpha\beta\beta}$ or $\underline{\boldsymbol{Q}} = \underline{\underline{\boldsymbol{i}}} : \underline{\underline{\underline{\boldsymbol{R}}}}$. $\underline{\underline{\boldsymbol{i}}}$ is the identity for in-plane tensor: $i_{\alpha\beta\gamma\delta} = \frac{1}{2}\left(\delta_{\alpha\gamma}\delta_{\beta\delta} + \delta_{\alpha\delta}\delta_{\beta\gamma}\right)$ where $\delta_{\alpha\beta}$ is the Kronecker symbol $\delta_{\alpha\beta} = 1$ if $\alpha = \beta$ and 0 if $\alpha \neq \beta$.

In the case of highly anisotropic laminated plates the distinction between every compononents of the gradient of the bending moment is necessary for deriving good estimate of the deflection and local transverse shear distribution through the thickness [6].

The full bending gradient $\underline{\underline{\underline{\boldsymbol{R}}}}$ has six components whereas $\underline{\boldsymbol{Q}}$ has two components. Thus, using the full bending gradient as static unknown introduces four additional static unknowns. More precisely: R_{111} and R_{222} are respectively the cylindrical bending part of shear forces Q_1 and Q_2, R_{121} and R_{122} are respectively the torsion part of these shear forces and R_{112} and R_{221} are linked to strictly self-equilibrated stresses.

Thus, from generalized stress definition (Eq. 1), the 3D equilibrium equations $\sigma_{ij,j} = 0$ are rewritten:

$$\begin{cases} R_{\alpha\beta\gamma} = M_{\alpha\beta,\gamma} \\ R_{\alpha\beta\beta,\alpha} + p_3 = 0 \end{cases} \iff \begin{cases} \underline{\underline{\underline{\boldsymbol{R}}}} = \underline{\underline{\boldsymbol{M}}} \otimes \underline{\underline{\boldsymbol{\nabla}}} \\ \left(\underline{\underline{\boldsymbol{i}}} : \underline{\underline{\underline{\boldsymbol{R}}}}\right) \cdot \underline{\underline{\boldsymbol{\nabla}}} + p_3 = 0 \end{cases} \text{ on } \omega \quad (2)$$

where p_3 is the out-of-plane load (cf *Fig. 1*).

Generalized stresses $\underline{\underline{\boldsymbol{M}}}$ and $\underline{\underline{\underline{\boldsymbol{R}}}}$ work respectively with the associated strain variables: $\underline{\underline{\boldsymbol{\chi}}}$, the curvature and $\underline{\underline{\underline{\boldsymbol{\Gamma}}}}$, the generalized shear strain. These strain fields must comply with compatibility equations:

$$\begin{cases} \Gamma_{\alpha\beta\gamma} = \Phi_{\alpha\beta\gamma} + i_{\alpha\beta\gamma\delta} U_{3,\delta} \\ \chi_{\alpha\beta} = \Phi_{\alpha\beta\gamma,\gamma} \end{cases} \iff \begin{cases} \underline{\underline{\underline{\boldsymbol{\Gamma}}}} = \underline{\underline{\underline{\boldsymbol{\Phi}}}} + \underline{\underline{\boldsymbol{i}}} \cdot \underline{\underline{\boldsymbol{\nabla}}} U_3 \\ \underline{\underline{\boldsymbol{\chi}}} = \underline{\underline{\underline{\boldsymbol{\Phi}}}} \cdot \underline{\underline{\boldsymbol{\nabla}}} \end{cases} \text{ on } \omega \quad (3)$$

where $\underset{\frown}{\boldsymbol{\Phi}}$ is the third-order tensor related to generalized rotations and U_3 is the average out-of-plane displacement. $\underset{\frown}{\boldsymbol{\Phi}}$ and $\underset{\frown}{\boldsymbol{\Gamma}}$ are 2D-third-order tensors following the symmetry $\Gamma_{\alpha\beta\gamma} = \Gamma_{\beta\alpha\gamma}$.

2.2.2 Bending-Gradient constitutive equations

Assuming full uncoupling between $\underset{\frown}{\boldsymbol{R}}$ and $\underset{\sim}{\boldsymbol{M}}$, the Bending-Gradient plate constitutive equations are:

$$\left\{ \begin{array}{l} M_{\alpha\beta} = D_{\alpha\beta\gamma\delta}\chi_{\delta\gamma} \\ \Gamma_{\alpha\beta\gamma} = f_{\alpha\beta\gamma\delta\varepsilon\zeta}R_{\zeta\varepsilon\delta} \end{array} \right. \Longleftrightarrow \left\{ \begin{array}{l} \underset{\sim}{\boldsymbol{M}} = \underset{\approx}{\boldsymbol{D}} : \underset{\sim}{\boldsymbol{\chi}} \\ \underset{\frown}{\boldsymbol{\Gamma}} = \underset{\frown}{\boldsymbol{f}} \vdots \underset{\frown}{\boldsymbol{R}} \end{array} \right. \text{ on } \omega \tag{4}$$

where $\underset{\approx}{\boldsymbol{D}} = \underset{\approx}{\boldsymbol{d}}^{-1}$ is the conventional Kirchhoff-Love fourth-order bending tensor classically defined as follows:

$$D_{\alpha\beta\gamma\delta} = \int_{-\frac{h}{2}}^{\frac{h}{2}} x_3^2 C^{\sigma}_{\alpha\beta\gamma\delta}(x_3)\, dx_3 \qquad \text{where } C^{\sigma}_{\alpha\beta\gamma\delta} = C_{\alpha\beta\gamma\delta} - \frac{C_{\alpha\beta 33}C_{\gamma\delta 33}}{C_{3333}}$$

$\underset{\approx}{\boldsymbol{C}}^{\sigma}$ is the plane stress elasticity tensor and $\underset{\approx}{\boldsymbol{C}} = \underset{\approx}{\boldsymbol{S}}^{-1}$ is the fourth-order 3D elasticity stiffness tensor. $\underset{\frown}{\boldsymbol{f}}$ is the sixth-order generalized shear compliance tensor defined as follows:

$$\underset{\frown}{\boldsymbol{f}} = \int_{-\frac{h}{2}}^{\frac{h}{2}} \left(\int_{\frac{-h}{2}}^{x_3} z \underset{\approx}{\boldsymbol{d}} : \underset{\approx}{\boldsymbol{C}}^{\sigma} dz \right) \cdot \underset{\sim}{\boldsymbol{g}} \cdot \left(\int_{\frac{-h}{2}}^{x_3} z \underset{\approx}{\boldsymbol{d}} : \underset{\approx}{\boldsymbol{C}}^{\sigma} dz \right) dx_3 \tag{5}$$

where $g_{\alpha\beta} = 4S_{\alpha 3\beta 3}$ is the out-of-plane Reissner shear compliance tensor. The fourth-order tensor $\underset{\approx}{\boldsymbol{D}}$ and the sixth order tensor $\underset{\frown}{\boldsymbol{f}}$ follow the major symmetry: $D_{\alpha\beta\gamma\delta} = D_{\delta\gamma\beta\alpha}$, $f_{\alpha\beta\gamma\delta\varepsilon\zeta} = f_{\zeta\varepsilon\delta\gamma\beta\alpha}$ and the minor symmetry: $D_{\alpha\beta\gamma\delta} = D_{\beta\alpha\gamma\delta}$, $f_{\alpha\beta\gamma\delta\varepsilon\zeta} = f_{\beta\alpha\gamma\delta\varepsilon\zeta}$.

2.2.3 A Projection of the Bending-Gradient model on a Reissner model

In the case of homogeneous plates, it has been demonstrated that the Bending-Gradient model strictly reduces to a Reissner model [5]. Indeed, it can be shown that $f_{\alpha\beta\gamma\delta\varepsilon\zeta} = i_{\alpha\beta\gamma\eta} f^R_{\eta\theta} i_{\theta\delta\varepsilon\zeta}$ where the second-order shear compliance tensor is classically defined as $f^R_{\alpha\beta} = \frac{6}{5} h S_{\alpha 3\beta 3}$ in the FOSDT. For this reason, the Bending-Gradient theory can be seen as an extension to heterogeneous plates of the Reissner theory.

Thus, from assumptions on Bending-Gradient generalized shear variables as a function of Reissner shear variables, several projections (or reduction) of the Bending-Gradient theory can be done on a Reissner model. Following this idea, Lebée and Sab [5] suggested the form $\underset{\frown}{\boldsymbol{R}} = \frac{2}{3} \underset{\approx}{\boldsymbol{i}} \cdot \underset{\sim}{\boldsymbol{Q}}$ for shear forces, reducing the number of shear stress variables from six to two. Mechanically, it is equivalent to assume that pure warping in the plate does not generate any stress. From this assumption, the projection of the sixth-order generalized shear tensor $\underset{\frown}{\boldsymbol{f}}$ is defined as follows [6]:

$$\underset{\sim}{\boldsymbol{f}}^R = \frac{4}{9} \begin{pmatrix} f_{111111} + f_{122221} + 2f_{111221} & 0 \\ 0 & f_{222222} + f_{121121} + 2f_{121222} \end{pmatrix}$$

This projection is used by Lebée and Sab to evaluate the distance between Bending-Gradient and Reissner-Mindlin models on bending problem in [5, 6].

2.2.4 Simple support boundary conditions

On the plate boundaries $\partial\Omega$, the normal and the in-plane tangent vectors are respectively noted $\underset{\sim}{\boldsymbol{n}}$ and $\underset{\sim}{\boldsymbol{t}}$. In timber construction, it is common to model boundaries by simply-supported edges [7]. In Reissner model, this boundary conditions consists in blocking the out-of-plane displacement U_3 and the transverse rotation φ_t. In the Bending-Gradient theory, boundary conditions are given by:

$$\underset{\sim}{\boldsymbol{M}} \text{ or } \underset{\frown}{\boldsymbol{\Phi}} \cdot \underset{\sim}{\boldsymbol{n}}$$
$$\left(\underset{\approx}{\boldsymbol{i}} \vdots \underset{\frown}{\boldsymbol{R}}\right) \cdot \underset{\sim}{\boldsymbol{n}} \text{ or } U_3$$

Thus, at boundaries, the bending moment M_{nt} is linked to the generalized rotation Φ_{ntn} whereas it is linked to φ_t in the Reissner model. By analogy, the simple support boundary conditions are defined as $\Phi_{ntn} = 0$ and $U_3 = 0$ in the Bending-Gradient model. Moreover, the over bending moments M_{nn} and M_{tt} are set to zero, as M_{nn} in the Reissner model.

2.3 Linear buckling analysis

2.3.1 Resolution with the Bending-Gradient theory

We assume that the plate is uniformly pre-loaded with the membrane stress $\underset{\sim}{\boldsymbol{N}}(\lambda) = \lambda \boldsymbol{e}_1 \otimes \boldsymbol{e}_1$. In linear buckling analysis, for some values of λ, one or several non-trivial equilibrium states, called buckling modes, are admissible. Although there is no external load p_3 in the equilibrium (Eq. 2) during buckling, an apparent one p_N is involved due to second-order effects of in-plane load $\underset{\sim}{\boldsymbol{N}}$ and to out-of plane deflection U_3. For Kirchhoff-Love plates and Reissner plates, it takes the classical form of:

$$p_N = -N_{\alpha\beta} U_{3,\alpha\beta} \quad [2]$$

We assume here that it is also applicable to the Bending-Gradient model since this theory is an extension of Reissner model to the case of heterogeneous plates. Thus, in (Eq. 2), the second equation of equilibrium becomes:

$$i_{\delta\gamma\varepsilon\zeta} R_{\zeta\varepsilon\gamma,\delta} - U_{3,\alpha\beta} N_{\alpha\beta} = 0 \qquad \Leftrightarrow \qquad \left(\underset{\approx}{\boldsymbol{i}} \vdots \underset{\sim}{\boldsymbol{R}}\right) \cdot \underline{\nabla} - (\underline{\nabla} \otimes \underline{\nabla} U_3) : \underset{\sim}{\boldsymbol{N}} = 0 \qquad \text{on } \omega \qquad (6)$$

The simplification of the set of equilibrium (Eq. 2, 6), compability (Eq. 3) and constitutive equations (Eq. 4) results in an eigenvalue problem which solutions are critical buckling modes λ associated with the corresponding eigenmodes $(U_3, \underset{\frown}{\boldsymbol{\Phi}})$:

$$\begin{cases} \underset{\approx}{\boldsymbol{i}} \vdots \left[\left(\underset{\approx}{\boldsymbol{D}} : (\underset{\frown}{\boldsymbol{\Phi}} \cdot \underline{\nabla}) \right) \otimes \underline{\nabla} \right] \cdot \underline{\nabla} - \lambda U_{3,11} = 0 \\ \underset{\frown}{\boldsymbol{\Phi}} + \underset{\approx}{\boldsymbol{i}} \cdot \underline{\nabla} U_3 = \underset{\frown}{\boldsymbol{f}} \vdots \left[\left(\underset{\approx}{\boldsymbol{D}} : (\underset{\frown}{\boldsymbol{\Phi}} \cdot \underline{\nabla}) \right) \otimes \underline{\nabla} \right] \end{cases} \quad \text{on } \omega \qquad (7)$$

This problem is solved, looking for expressions of U_3 and $\underset{\frown}{\boldsymbol{\Phi}}$ in the form of Fourier-like series. Considering kinematic compatibility (Eq. 3), simple support boundary conditions and the geometry of the plate, which is rectangular with each layer's principal axes coinciding with rectangular reference frame $(\boldsymbol{e}_1, \boldsymbol{e}_2, \boldsymbol{e}_3)$, expressions of U_3 and $\underset{\frown}{\boldsymbol{\Phi}}$ are looked in the following form:

$$U_3 = \sum_{m=1}^{\infty} \sum_{n=1}^{\infty} U_3^{mn} \sin(K_m x_1) \sin(K_n x_2)$$

$$\Phi_{\alpha\beta\gamma} = \sum_{m=1}^{\infty} \sum_{n=1}^{\infty} \Phi_{\alpha\beta\gamma}^{mn} \cos(K_m x_1) \sin(K_n x_2) \quad \text{for } \Phi_{111}, \Phi_{221} \text{ and } \Phi_{122}$$

$$\Phi_{\alpha\beta\gamma} = \sum_{m=1}^{\infty} \sum_{n=1}^{\infty} \Phi_{\alpha\beta\gamma}^{mn} \sin(K_m x_1) \cos(K_n x_2) \quad \text{for } \Phi_{121}, \Phi_{112} \text{ and } \Phi_{222}$$

$$\text{where } K_m = \frac{m\pi}{a} \text{ and } K_n = \frac{n\pi}{b} \text{ for } \{m,n\} \in \mathbb{N}^{*2}$$

U_3^{mn} and $\Phi_{\alpha\beta\gamma}^{mn}$ are respectively the amplitudes of each term of the out-of-plane displacement and the generalized rotations associated with the $\{m,n\}$ mode.

These expressions are injected in the buckling problem (Eq. 7). It is noticed from the orthogonality of the series, that each equation is satisfied only if it is satisfied for each individual term in cosine and sine series. Thus all harmonic functions can be omitted in the following developments.

Solutions of the buckling problem are then eigenmodes $\left(U_3^{mn}, \Phi_{\alpha\beta\gamma}^{mn}\right)$ associated with the corresponding eigenvalue λ_{mn}. Here, we are only interested in the lowest value λ_{mn} among all $\{m,n\} \in \mathbb{N}^2$. The lowest mode $\{m,n\}$ depends on the plate aspect ratio $\frac{a}{b}$, the plate slenderness $\frac{b}{h}$ and the material characteristics. In the studied domain, namely $\frac{a}{b} \in [0.5, 2]$ and $\frac{b}{h} \in [10, 35]$, with material characteristics given in *Tab. 1*, it can be demonstrated that the lowest eigenvalue is always λ_{11} or λ_{21} (cf Section 4.2).

3 3D reference model for CLT

A 3D numerical study is performed using the finite element software ABAQUS. These numerical results will be consider as the reference results for the comparison with analytical results in section 4.

3.1 Characteristics of the 3D problem

3.1.1 External load

On the sides, uniform displacements perpendicular to the faces are applied. These displacements are chosen so that uniform membrane strains appear in the plate. This is insured by choosing the displacement on boundaries $\partial\Omega_2$ $(x_2 = \{0, b\})$ which corresponds to average Poisson effects in the plate. Practically, for a choosen displacement $u_1 = a_{1111}\frac{a}{2}$ on $\partial\Omega_1$ $(x_1 = \{0, a\})$, a displacement of $u_2 = a_{1122}\frac{b}{2}$ on $\partial\Omega_2$ will vanish the N_{12} and N_{22} components and set $N_{11} = 1$ because of:

$$\frac{1}{2}\left(U_{\alpha,\beta} + U_{\beta,\alpha}\right) = a_{\alpha\beta\gamma\delta}N_{\gamma\delta} \Leftrightarrow (\underline{\boldsymbol{U}} \otimes^s \underline{\boldsymbol{\nabla}}) = \underset{\approx}{\boldsymbol{a}} : \underset{\sim}{\boldsymbol{N}} \qquad \text{with } \underset{\approx}{\boldsymbol{a}}^{-1} = \underset{\approx}{\boldsymbol{A}} = \int_{-\frac{h}{2}}^{\frac{h}{2}} \underset{\approx}{\boldsymbol{C}}^{\sigma} dx_3 \tag{8}$$

$\underline{\boldsymbol{U}}$ is the average in-plane displacement and $\underset{\approx}{\boldsymbol{A}}$ the membrane stress tensor.

3.1.2 Simple support boundary conditions

Simple support boundary conditions (cf Section 2.2.4) applied on the 2D plate models can not be transposed directly to 3D problems. Indeed in 3D, there are no rotation fields $\underline{\boldsymbol{\varphi}}$ but only three translationnal degrees of freedom. Blocking the transverse displacements is a good 3D modelisation to set transverse rotation φ_t to zero. Indeed, in a pure bending problem, in-plane displacements are negligible. Setting $u_t = 0$ on boundaries in a 3D problem has thus few influence on in-plane displacements but it prevents from transverse rotation on boundaries.

In linear buckling analysis, it is however necessary to consider two steps: the pre-loading used for the evaluation of the geometric stiffness matrix, and the eigenvalue problem for the determination of the buckling modes. During the first step, the problem is only a membrane problem: there are only in-plane displacements u_α and no rotations φ_α. Thus, setting $u_t = 0$ on boundaries is not necessary and will only prevent from in-plane Poisson's effect on boundaries: only the simple support boundary condition $u_3 = 0$ is thus set during this step. The second step is essentially an out-of-plane problem, it is comparable with plate bending. Thus, setting $u_t = 0$ and $u_3 = 0$ on boundaries is a good modelisation of simple support conditions.

3.1.3 Definition of the numerical model

The C3D8 element, a 3D brick-element with 8 nodes is used to mesh the plate. There are three degrees of freedom at each node, one for each translation. A linear interpolation is used in each direction. A full integration is done at each node to evaluate the material response in each element. A convergence study has been performed to find the most suitable mesh with an accuracy of 1%.

3.1.4 Timber elastic characteristics and CLT configurations

Timber is a material with a high anisotropy which is often modeled as a linear orthotropic material. Norway Spruce mechanical caracteristics are used in the present paper because it is one of the most used species in timber construction. References values will be taken from Keunecke *et al* [8]. Young modulus is defined by the ratio between tensile stress and tensile strain $E_i = \frac{\sigma_{ii}}{\varepsilon_{ii}}$ for a traction in the i-direction. The shear modulus is defined by the ratio between shear stress and shear strain $G_{ij} = \frac{\sigma_{ij}}{\varepsilon_{ij}}$ for a pure shear between i and j-directions. The Poisson's ratio is defined as the ratio between contraction and elongation $\nu_{ij} = \frac{\varepsilon_{jj}}{\varepsilon_{ii}}$ for a traction in i-direction. In order to model an orthotropic material, shear

compliance terms $S_{RRTT} = \frac{\nu_{TR}}{E_T}$ and $S_{TTRR} = \frac{\nu_{RT}}{E_R}$ are averaged to comply with $\underset{\approx}{\boldsymbol{S}}$ major symmetry. From these new expressions of $S^m_{RRTT} = S^m_{TTRR}$, ν^m_{RT} and ν^m_{TR} are calculated to get an orthotropic material.

$\mathbf{E_L}$	E_R	E_T	G_{LR}	G_{LT}	$\mathbf{G_{RT}}$	ν_{LR}	ν_{RL}	ν_{LT}	ν_{TL}	ν^m_{RT}	ν^m_{TR}
12800	625	397	617	587	**53**	0.36	0.018	0.45	0.014	0.41	0.26

Tab. 1: Elastic Properties of Norway Spruce, E and G in MPa [8]

There is a high contrast between the longitudinal stiffness E_L and the rolling shear stiffness G_{RT}. These two characteristics will thus arise the buckling of CLT panels. For this reason, the influence of the orientations of radial and tangential directions, which are turning in actual lumbers, is negligible. In the present model, R is chosen in out-of-plane direction and the longitudinal-tangential plane has alternatively an angle of 0°or 90°with the mid-plane $\left(O, \boldsymbol{e}_3\right)$ depending on layers. Outer layers fibers are oriented in x_1-direction. Each ply is crossed of a 90°angle with adjacent plies.

In the following, the ratio between the width of the loaded edge b and the thickness of the plate h, called the slenderness $\frac{b}{h}$, varies between 10 and 35 and the plate aspect $\frac{a}{b}$, the ratio between the length and the width of the plate, varies between 0.5 and 2 according to the geometries of actual structures.

3.2 3D buckling of CLT panels

3.2.1 Buckling load and compressive strength

The buckling load and the compressive strength of CLT panels are of the same order of magnitude. Indeed, from the paper of Cabrero *et al.* [9], the average strength of timber in compression is 41.7MPa. For a 5-ply CLT, we may assume that only the three longitudinal plies are working in compression. Thus the compressive strength of a 5-ply CLT panel may be set as $41.7 \times \frac{3}{5} \approx 25$MPa and does not vary with $\frac{b}{h}$ and $\frac{a}{b}$ contrary to the buckling load. As an example, for a 5-ply CLT square panel with a slenderness $\frac{b}{h} = 25$, buckling occurs at 18.1MPa, before plasticity (cf Fig. 3). This remark shows the necessity to take into account instabilities to design CLT structures.

3.2.2 Behavior of a CLT panel across thickness

On *Fig. 2*, the displacement u_1 is plotted on the loaded edge for a 5-ply CLT panel: displacements u_1 are voluntary deformed twice more than in other directions. Its amplitude is around one tenth of the out-of-plane deflection amplitude: in-plane displacement are not negligible.

The displacement u_1 is not linear across thickness, and thus the shear strain ε_{13} is not uniform along x_3. The section of the plate doesn't remain plane during buckling because of the warping between longitudinal layers and cross layers. Indeed, longitudinal layers are stiffer than cross layers in the x_1-direction. During buckling, longitudinal layers are the most loaded plies. The upper fiber, $x_3 = \frac{h}{2}$, is tensed whereas the lower fiber, $x_3 = -\frac{h}{2}$, is compressed due to the bending of the plate. Since the cross layers are softer, they do not bent as longitudinal layers. The section of cross layers remains approximately vertical even during buckling. This phenomenon is well-known in sandwich structures where skins work essentially in bending whereas the out-of-plane shear stress acts essentially on the core of the sandwich panel.

In the Bending-Gradient theory, several variables are used to describe this phenomenon. On one side, Φ_{111} is related to the global rotation of the section. In the same way, Γ_{111} is linked to the global shear of the plate which comes from the difference between the global rotation of the plate and the first derivation of the deflection $u_{3,1}$. On the other side, $\Phi_{221} = \Gamma_{221}$ is related to the warping between layers. These distinctions between rotation, warping and their derivation can obviously not be fully captured by a Reissner model with only one variable φ_1 in the x_1-direction. Qualitatively, the Bending-Gradient describes better the behavior of CLT panels. Numerical results in section 4 will support this observation.

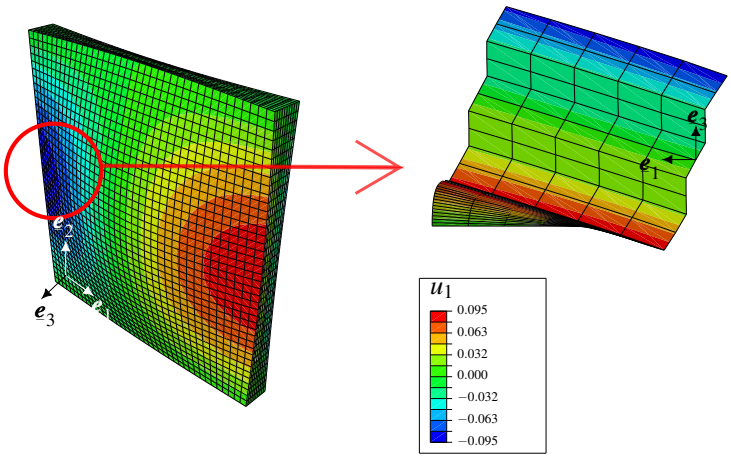

Fig. 2: Displacement u_1 according to thickness on $(x_1 = -a/2) \cap (x_2 = 0)$

4 Comparison between numerical results and plate models

In the following, the application of the Bending-Gradient to the linear plate buckling is compared to classical models of Kirchhoff-Love and Reissner. For the latter, the well-known FOSDT with the shear correction factor $\kappa = \frac{5}{6}$ is plotted as well as the projection of the Bending-Gradient on the Reissner model suggested in Section 2.2.3. Finally the 3D numerical calculation by finite element is used as reference to compare the accuracy of each theory.

4.1 Results for a square plate

Fig.3 represents the first buckling load of a 5-ply square CLT panel plotted along slenderness $\frac{b}{h}$. As expected, the Kirchhoff-Love model gives results far from the actual ones: the error is even higher than 15% for a slenderness $\frac{b}{h} \leq 25$. The classical FOSDT, by considering shear effects, is more precise than the Kirchhoff-Love model. However, the error is still high. In the studied domain, the Bending-Gradient theory is clearly the model which best describes the buckling load of plates. For slenderness $\frac{b}{h} > 10$, the error is less than 2.5%, and for $\frac{b}{h} > 13$ the order of magnitude of the error is equivalent to the precision of numerical results.

It is finally noticed that the projection on a Reissner model gives almost same results as the full Bending-Gradient model: the difference is around 0.1%. Using the Bending-Gradient directly seems not necessary in this case since the gain of precision compared to its projection is negligible compared to the difficulty introduced by generalizing the shear stresses.

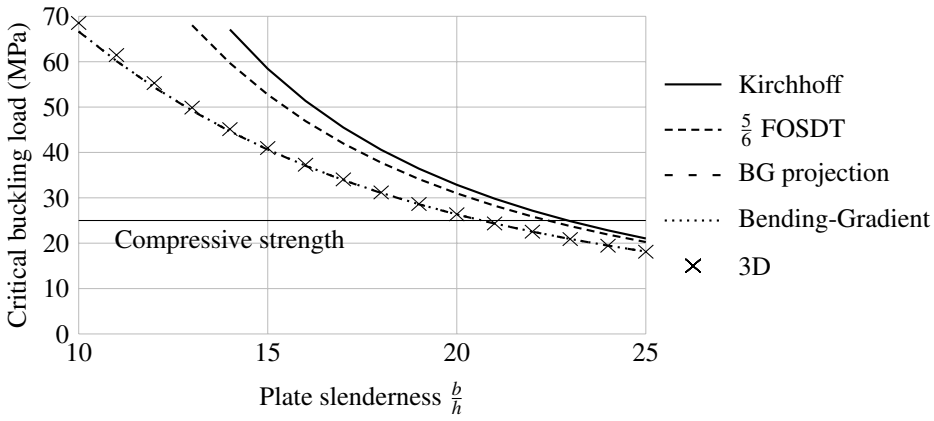

Fig. 3: Buckling load according to slenderness $\frac{b}{h}$ for a 5ply-CLT square panel

Moreover the buckling load is lower than the compressive strength for slenderness $\frac{b}{h} \geq 21$ in actual structures. Thus, CLT walls may buckle before the compression failure occurs which leads to

the necessity to design these panels to prevent buckling. Furthermore the high sensibility to defects of the buckling compared to bending increases the risk of instabilities of actual structures.

On *Fig. 4*, the relative error of plate models is plotted for 3-ply CLT panels which are more slender: the slenderness domain here is higher than in 5-ply CLT since the thickness of each ply is technologically limited to 4 centimeters. For 3-ply CLT panels, the relative error of classical Kirchhoff theory and FOSDT is still high even for relatively slender structures in CLT. On the contrary, the Bending-Gradient theory and its projection are close to the 3D solution in all the studied domain with an accuracy with the same amplitude as the precision of numerical results.

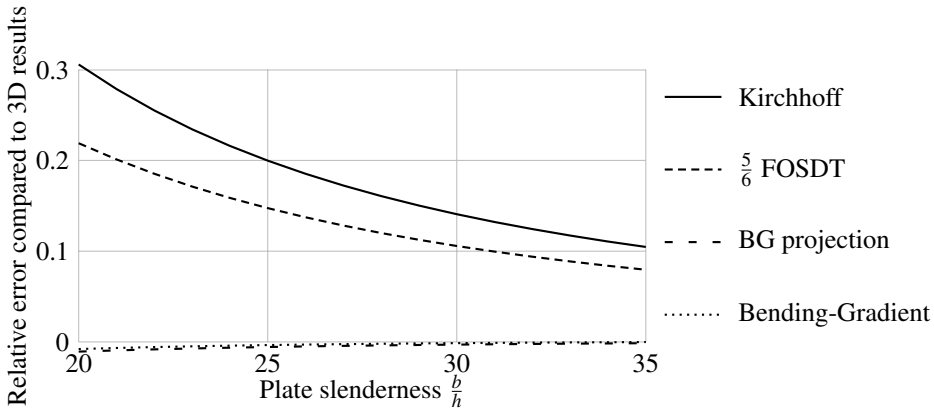

Fig. 4: Relative error of plate models compared to 3D results for a 3ply-CLT square panel

4.2 Variation of the plate aspect ratio $\frac{a}{b}$

Fig. 5 represents the buckling load of a 5-ply CLT with a slenderness $\frac{b}{h} = 20$ for a varying plate aspect ratio. There are here successively two eigenmodes: $(m = 1, n = 1)$ and $(m = 2, n = 1)$. Quantitatively, the same results as previously are obtained: the Bending-Gradient theory and its projection are very accurate contrary to more classical models. This figure shows that the Bending-Gradient is still accurate when varying aspect ratio and even for several eigenmodes.

Moreover, the critical load and the compressive strength have close values for aspect ratios between 1.0 and 1.5 which confirms the necessity of the development of a new engineering tool to design the CLT panels against buckling. The Bending-Gradient's projection on the Reissner theory could be an appropriate model to create this tool.

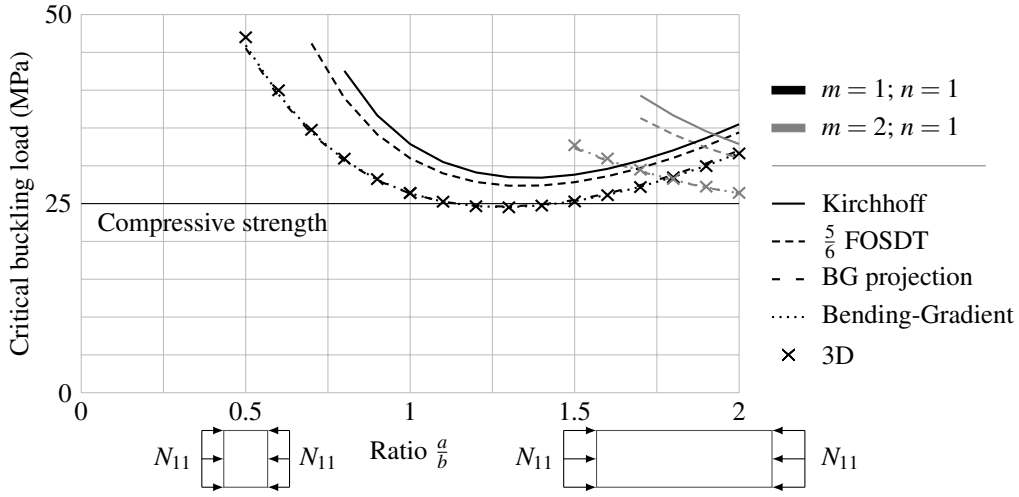

Fig. 5: Buckling load according to plate ratio $\frac{a}{b}$ for 5ply-CLT with slenderness $\frac{b}{h} = 20$

5 Conclusions

In this paper, the Bending-Gradient theory has been extended to the buckling analysis which has been applied to the case of rectangular plates. A projection of this theory on a Reissner model has also been presented. A 3D numerical study has been conducted in order to get reference results for the buckling of CLT panels. Results have shown that, qualitatively and quantitatively, the Bending-Gradient is well adapted for the study of the buckling of thick and highly anisotropic laminated plates such as CLT contrary to the FOSDT and the Kirchhoff model. Moreover, the suggested projection of the Bending-Gradient, proved to be also very accurate, seems thus more adapted than the full Bending-Gradient theory to engineering issues since it uses a simpler model, the Reissner model, without loosing accuracy. Indeed, this projection could be used to create a new engineering tool for the design of CLT buckling. To this end, imperfections of actual structures and variability of the timber characteristics, in particular the rolling shear stiffness which is not considered in the Eurocode 5, have to be investigated in a further work. To be complete, creep should also be studied to evaluate the influence of permanent loading across time.

References

[1] G. Kirchhoff,Über das Gleichgewicht und die Bewegung einer elastischen Scheibe. *Journal für die reine und angewandte Mathematik*, 40: 51-88, 1850 (German)

[2] S. Timoshenko, S. Woinowsky-Krieger, Theory of elastic stability. Second Edition. *McGraw-Hill Book Company*, 1987

[3] E. Reissner, The effect of transverse shear deformation on the bending of elastic plates. *Journal of Applied Mechanics* 12, 68-77, 1945

[4] H. Murakami, Laminated composite plate theory with improved in-plane responses, *Journal of Applied Mechanics*, Vol. 53 661-666, September 1986

[5] A. Lebée, K. Sab, A Bending-Gradient model for thick plates, Part I : Theory. *International Journal of Solids and Structures* 48 2878-2888, 2011

[6] A. Lebée, K. Sab, A Bending-Gradient model for thick plates, Part II : Closed-form solutions for cylindrical bending of laminates. *International Journal of Solids and Structures* 48 2889-2901, 2011

[7] Dujic, B., Aicher, S., Zarnič, R. (2005)Investigations on in-plane loaded wooden elements - influence of loading and boundary conditions. *Otto-Graf-Journal*, Vol.16, 259-272.

[8] D. Keunecke, S. Hering, P. Niemz, Three-dimensional elastic behaviour of common yew and Norway spruce. *Wood Science and Technology* 42:633-647, 2008

[9] J. M. Cabrero, C. Blanco, K. G. Gebremedhin, A. Martin-Meizoso, Assessment of phenomenological failure criteria for wood. *European Journal of Wood and Wood Products*, Volume 70, Issue 6, pp 871-882, 2012